

Impact of Mass Generation for Simplified Dark Matter Models

Nicole F. Bell, Yi Cai and Rebecca K. Leane

ARC Centre of Excellence for Particle Physics at the Terascale
School of Physics, The University of Melbourne, Victoria 3010, Australia

E-mail: n.bell@unimelb.edu.au, yi.cai@unimelb.edu.au,
rleane@physics.unimelb.edu.au

Abstract. In the simplified dark matter models commonly studied, the mass generation mechanism for the dark fields is not typically specified. We demonstrate that the dark matter interaction types, and hence the annihilation processes relevant for relic density and indirect detection, are strongly dictated by the mass generation mechanism chosen for the dark sector particles, and the requirement of gauge invariance. We focus on the class of models in which fermionic dark matter couples to a spin-1 vector or axial-vector mediator. However, in order to generate dark sector mass terms, it is necessary in most cases to introduce a dark Higgs field and thus a spin-0 scalar mediator will also be present. In the case that all the dark sector fields gain masses via coupling to a single dark sector Higgs field, it is mandatory that the axial-vector coupling of the spin-1 mediator to the dark matter is non-zero; the vector coupling may also be present depending on the charge assignments. For all other mass generation options, only pure vector couplings between the spin-1 mediator and the dark matter are allowed. If these coupling restrictions are not obeyed, unphysical results may be obtained such as a violation of unitarity at high energies. These two-mediator scenarios lead to important phenomenology that does not arise in single mediator models. We survey two-mediator dark matter models which contain both vector and scalar mediators, and explore their relic density and indirect detection phenomenology.

Contents

1	Introduction	1
2	Mass Generation for Spin-1 Simplified Models	3
3	Scenario I: Bare DM Mass and Z' Mass from Stueckelberg Mechanism	5
3.1	Model	5
4	Scenario II: DM Mass and Z' Mass both from Dark Higgs Mechanism	5
4.1	Model	5
4.2	Cross Sections	7
4.3	Relic Density	8
5	Scenario III: DM Mass from Dark Higgs Mechanism, Z' Mass from Stueckelberg Mechanism	9
5.1	Model	10
5.2	Cross Sections	10
5.3	Relic Density	11
6	Scenario IV: Bare DM Mass, Z' Mass from Dark Higgs Mechanism	13
6.1	Model	13
6.2	Cross Sections	13
6.3	Relic Density	13
7	Indirect Detection Phenomenology	14
8	Discussion and Summary	17
A	Cross Sections	18

1 Introduction

The search for particle interactions of dark matter (DM) is currently being pursued across a great variety of experiments. Foremost amongst these are the searches for Weakly Interacting Massive Particles (WIMPs) [1, 2]. The WIMP mass and coupling parameters are being probed with unprecedented sensitivity at in direct detection experiments such as LUX [3, 4] and PandaX-II [5], the mono- X searches at the Large Hadron Collider [6–35], and in indirect detection analysis of astrophysical gamma-ray fluxes such as those measured by the Fermi-LAT satellite [36]. The physics reach of these searches is such that we can realistically expect to cover much of the WIMP parameter space in the near future. As such, it is imperative to have well-formulated models of DM interactions which span a comprehensive spectrum of possible interaction types, in a manner which is as model independent as possible. Simplified models address this aim by introducing a single DM candidate and a mediator which communicates between the dark and SM sectors [37–44]. The three most commonly considered benchmark simplified models involve the interaction of fermionic DM with Standard Model

(SM) fermions via a spin-1 s -channel mediator, a spin-0 s -channel mediator, or a spin-0 t -channel mediator [42].

These simplified models are an improvement over the effective field theory approach [26, 45, 46] which was used for many recent collider and non-collider WIMP searches, yet suffers from unitarity issues when used outside the region of validity [47–57]. However, the simplified models are still far from ideal. Indeed, by their simplified nature, they are not intrinsically capable of capturing the realistic phenomenology of many UV complete theories, which may have multiple dark-sector field content. More critically, separate consideration of the benchmark simplified models can lead to scenarios that are not physically viable. Indeed, the simplified models suffer some of the same issues that plague the effective field theory approach, such as violations of perturbative unitarity that arise because gauge invariance is not respected [23, 47–60].

As an example of such an issue, simplified models in which the DM has a non-zero axial-vector coupling to a spin-1 mediator will violate perturbative unitarity at high energies [58, 61]. This can be remedied by introducing a dark Higgs field to unitarize the longitudinal component of the Z' [58, 61–63]. The dark Higgs may also provide mass to the DM itself. The minimal self-consistent approach is then a multi-mediator model, featuring both spin-1 and spin-0 mediators¹. This of course can alter the phenomenology, even at low energies. In our recent work [62], we considered indirect detection signals in a scenario with a Majorana DM candidate χ , in which the couplings of a Z' and scalar, s , are related by gauge invariance. In this scenario, the presence of both the s and Z' mediators opens a dominant s -wave annihilation channel, $\chi\chi \rightarrow sZ'$, that does not arise when a single-mediator is considered in isolation [62]. This has a dramatic impact on the indirect detection phenomenology.

An important consideration for DM models is the mass generation mechanism for the dark sector fields. Although commonly left unspecified in the simplified model approach, with mass terms simply added by hand, we shall argue that the mechanism of mass generation has significant consequences that cannot be ignored. For a spin-1 mediator with only vector couplings, a standard procedure is to appeal to the Stueckelberg mechanism to introduce a mass for the vector boson. However, this is valid only for a pure vector, with vanishing axial-vector couplings to fermions. This is a very specific scenario, and there is no reason to assume it is correct. In fact, the Higgs mechanism is the only mass generation mechanism we know is realized by nature, as confirmed by the recent experimental discovery of the SM Higgs boson. As such, it is well motivated to consider a variety of scenarios where different dark sector fields acquire their mass by various methods: the Stueckelberg mechanism, a dark Higgs mechanism, or in cases where it is allowed, simply with a bare mass term.

We will show that the annihilation processes, and hence both the relic density and indirect detection constraints, are strongly dictated by the mass generation mechanisms. Interestingly, we will also show that depending on the choice of mass generation mechanism, only particular interactions types are allowed, as dictated by dark gauge invariance. In most cases, only pure vector couplings of the spin-1 mediator to fermionic DM are allowed. Conversely, if a single dark Higgs mechanism gives mass to all the dark sector fields, the axial-vector coupling of the spin-1 mediator to the DM is required to be non-zero. Such restrictions do not map to the single-mediator simplified models, despite being a compelling possibility (or in some cases, a requirement). Again, this phenomenology is not accurately captured by the single mediator simplified model framework.

¹Multi-mediator models have also been considered recently in Refs. [62–66].

The purpose of this paper is to undertake a more complete study of simplified models that contain both a scalar and vector mediator. In all cases, we will be sure to enforce gauge invariance with respect to the dark $U(1)_\chi$ interaction (dark gauge invariance), which is important to ensure physically well behaved cross sections. We will consider Dirac DM, which allows for a wider combination of coupling types, each with their own distinct phenomenology. Results for Majorana DM can be obtained in the limit of one of the scenarios we investigate in this paper. We focus, in particular, on hidden-sector type models [67–92], where the DM annihilates directly to the mediators, which then decay to SM particles via small couplings between the dark and visible sectors. In section 2 we outline mass generation for spin-1 simplified models, and in section 3 we briefly discuss the standard assumption for mass generation in spin-1 models, before investigating three other compelling mass generation scenarios in sections 4, 5 and 6, detailing models, annihilation processes and relic density constraints. We present indirect detection constraints in section 7 and summarize our findings in section 8.

2 Mass Generation for Spin-1 Simplified Models

The mass generation mechanism for fermionic DM in spin-1 simplified models is tightly correlated with the DM interaction type. In the case that DM is Majorana, the Z' can have only axial-vector couplings to the DM, as vector couplings of Majorana particles vanish. In the case where DM is Dirac, both vector and axial-vector couplings to the Z' can simultaneously be present. For both DM types, the presence of an axial-vector coupling is significant, as it implies that

1. The DM mass must arise after symmetry breaking, as the $U(1)_\chi$ gauge symmetry prevents a bare mass term for χ , and
2. A $U(1)_\chi$ symmetry breaking mechanism is required to give the Z' mass, in order to unitarize the longitudinal component of the Z' .

A single dark Higgs field is an economical solution to these issues. In the following sections, we will show that the only scenario in which an axial-vector coupling is possible in a spin-1 mediator model is if there is a dark Higgs which interacts with both the DM and the dark gauge boson. Moreover, the axial coupling is not merely possible in this case, but in fact required to be non-zero by gauge invariance. We take the DM to be Dirac, as this permits the broadest range of possible coupling types. A related model involving Majorana fermions can be found in Ref. [62] and is closely related to a specific realization of scenario II presented below.

For Dirac DM, it is possible to have pure vectorlike couplings to the Z' and so it is possible to include a bare mass term for DM, and use the Stueckelberg mechanism² to provide a mass for the Z' , such that no dark Higgs is needed. Nonetheless, even in the case of pure vector couplings, a dark Higgs may still provide mass for one or both of the Z' and DM. Furthermore, when the Z' and DM masses arise from different mechanisms, the coupling of

²In Abelian gauge theories, the Stueckelberg mechanism can be taken as the limit of the Higgs mechanism where the mass of the real scalar is sent to infinity and only the pseudoscalar is present; however it is not always easily realized in more complicated scenarios. In particular, unitarity is already violated at tree-level in a non-Abelian theory with a Stueckelberg Lagrangian and thus the theory is not renormalizable [93–101]. In general the Stueckelberg mechanism should be treated as an alternative to the Higgs mechanism for mass generation.

Scenario	χ mass	Z' mass	Required $\chi - Z'$ coupling type	Annihilation processes	Z' pol
I	Bare mass term	Stueckelberg mechanism	Vector		Z'_T
II	Yukawa coupling to Dark Higgs	Dark Higgs mechanism	Vector & axial-vector or pure axial-vector. The $U(1)$ charge assignments of χ_L and χ_R determine the relative size of the V and A couplings. The axial-vector coupling must be non-zero.		Z'_T & Z'_L
III	Yukawa coupling to Dark Higgs	Stueckelberg mechanism	Vector		Z'_T
IV	Bare mass term	Dark Higgs mechanism	Vector		Z'_T

Table 1. The spectrum of scenarios with distinct phenomenology once mass generation is specified. All t -channel annihilation processes have an accompanying u -channel process which is not shown. All processes shown are s -wave, except for $\chi\bar{\chi} \rightarrow s \rightarrow Z'Z'$ diagram in scenario II, which while p -wave when considered alone, is part of the process $\chi\bar{\chi} \rightarrow Z'Z'$. For scenario III, as the dark Yukawa and gauge coupling are not correlated, the p -wave annihilation to two dark Higgs, $\chi\bar{\chi} \rightarrow ss$, can have an impact on the relic density if the gauge coupling is sufficiently small to suppress the s -wave processes. Otherwise, the s -wave processes shown dominate, even at freeze-out. The final column displays the polarization of the Z' bosons produced by these annihilation processes (in the $E_{Z'}^2 \gg m_{Z'}^2$ limit).

the DM to the scalar and vector mediators are no longer related to each other, and hence the phenomenology is less constrained. We are thus led to a spectrum of models in which both scalar and vector mediators would be present. We outline the phenomenologically distinct scenarios in Tab. (1).

3 Scenario I: Bare DM Mass and Z' Mass from Stueckelberg Mechanism

Interaction type required: Pure Vector

This is the most minimal gauge-invariant scenario, and is permitted only if there are pure vectors couplings between the DM and the Z' . Unlike the axial-vector scenario, a dark Higgs is not mandatory in the pure vector case because

1. The Z' gauge boson can acquire a mass via the Stueckelberg mechanism.
2. As χ is vectorlike with respect to the $U(1)_\chi$, i.e. $Q_{\chi_R} = Q_{\chi_L}$, a bare χ mass term is permitted.

3.1 Model

The Lagrangian for this case is simply

$$\mathcal{L} = \mathcal{L}_{SM} + i\bar{\chi}(\partial_\mu + ig_\chi Q_V Z'_\mu)\gamma^\mu\chi - \frac{\sin\epsilon}{2}Z'^{\mu\nu}B_{\mu\nu} - m_\chi\bar{\chi}\chi + \frac{1}{2}m_{Z'}^2 Z'^\mu Z'_\mu. \quad (3.1)$$

where Q_V is the vectorlike $U(1)_\chi$ charge of the DM, which can be chosen freely, and the ϵ term describes kinetic mixing of the $U(1)_\chi$ gauge boson with the SM hypercharge gauge boson. This is the only spin-1 mediator scenario where it is possible to avoid the inclusion of a dark Higgs. This case has been thoroughly covered in the literature (for a review see, e.g., [43]); we do not discuss it further.

4 Scenario II: DM Mass and Z' Mass both from Dark Higgs Mechanism

Interaction type required: Non-Zero Axial-Vector

We now consider the case where both the DM and the dark gauge boson acquire mass from a single dark Higgs. We will show that this requires the axial-vector DM- Z' interaction to be non-zero. The reason is simple: the dark Higgs field, S , must clearly carry $U(1)_\chi$ charge if its vacuum expectation value (vev) is to break that symmetry. A Yukawa coupling of the dark Higgs to the DM of the form $y_\chi\chi_R\chi_LS$ is then possible only if the DM is chiral, i.e. χ_L and χ_R carry different $U(1)_\chi$ charges. This guarantees that the axial coupling is non-zero (while the vector couplings may be either zero or non-zero depending on the $U(1)_\chi$ charge assignments).

4.1 Model

We investigate the phenomenology of the most minimal model containing a dark gauge boson and a dark Higgs field, by simply extending the Standard Model by an extra $U(1)$. The gauge group is thus: $SU(3)_c \otimes SU(2)_W \otimes U(1)_Y \otimes U(1)_\chi$. Here the covariant derivative is $D_\mu = D_\mu^{SM} + iQg_\chi Z'_\mu$, where Q denotes the $U(1)_\chi$ charge. The SM field content is augmented

by a Dirac fermion DM candidate, χ , a spin-1 dark gauge boson, Z' , and a dark Higgs field S . The vev of the dark Higgs field provides a mass generation mechanism for the dark sector fields Z' and χ . Before electroweak and $U(1)_\chi$ symmetry breaking, the most general Lagrangian is

$$\mathcal{L} = \mathcal{L}_{\text{SM}} + i\bar{\chi}_L \not{D}\chi_L + i\bar{\chi}_R \not{D}\chi_R - (y_\chi \bar{\chi}_R \chi_L S + h.c.) + (D^\mu S)^\dagger (D_\mu S) - \mu_s^2 S^\dagger S - \lambda_s (S^\dagger S)^2 - \lambda_{hs} (S^\dagger S)(H^\dagger H) - \frac{\sin \epsilon}{2} Z'^{\mu\nu} B_{\mu\nu}. \quad (4.1)$$

We assume that the SM fields are not charged under $U(1)_\chi$. There are thus only two possible terms that couple SM and dark-sector fields: the kinetic mixing of the $U(1)$ gauge boson with the hypercharge gauge boson, controlled by the kinetic mixing parameter ϵ , and mixing of the dark Higgs, S , with the SM Higgs, H , controlled by the Higgs mixing parameter λ_{hs} .

In order for the χ - S Yukawa term to be gauge invariant, the charges of the dark sector field must be chosen to satisfy³

$$Q_{\chi_R} - Q_{\chi_L} = Q_S. \quad (4.2)$$

We can set the dark Higgs charge to be $Q_S = 1$, without loss of generality, as any other choice can be absorbed into a rescaling of the dark gauge coupling. The χ charges therefore satisfy

$$Q_A \equiv \frac{1}{2}(Q_{\chi_R} - Q_{\chi_L}) = \frac{1}{2}, \quad (4.3)$$

$$Q_V \equiv \frac{1}{2}(Q_{\chi_R} + Q_{\chi_L}) = \frac{1}{2} + Q_{\chi_L}. \quad (4.4)$$

These charges determine the vector and axial-vector couplings of the Z' to the χ . We see that the axial-vector coupling is completely determined, while there is freedom to adjust the vector coupling by choosing $Q_{\chi_{L,R}}$ appropriately. For instance, $Q_{\chi_L} = 0$ would lead to equal vector and axial-vector couplings, while $Q_{\chi_L} \gg 1$ would lead to a vector coupling much larger than the axial-vector. Pure axial-vector is obtained with $Q_{\chi_L} = -1/2$; this produces phenomenology similar to the Majorana model studied in [62]. Pure vector, on the other hand, can only be approximately reached in the limit $Q_V \gg 1$, but never fully realized⁴, as dark gauge invariance prevents the axial-vector from being exactly zero.

Both S and H obtain vevs, breaking $SU(3)_c \otimes SU(2)_L \otimes U(1)_Y \otimes U(1)_\chi$ down to $SU(3)_c \otimes U(1)_{em}$. In the broken phase, the terms of interest are

$$\begin{aligned} \mathcal{L} \supset & -\frac{1}{2}m_s^2 s^2 + \frac{1}{2}m_{Z'}^2 Z'^\mu Z'_\mu - m_\chi \bar{\chi}\chi \\ & + g_\chi^2 w Z'^\mu Z'_\mu s - \lambda_s w s^3 - 2\lambda_{hs} h s(v s + w h) + g_f \sum_f Z'_\mu \bar{f} \Gamma_f^\mu f \\ & - g_\chi Q_V Z'_\mu \bar{\chi} \gamma^\mu \chi - g_\chi Q_A Z'_\mu \bar{\chi} \gamma^\mu \gamma_5 \chi - \frac{y_\chi}{\sqrt{2}} s \bar{\chi} \chi, \end{aligned} \quad (4.5)$$

³For anomaly cancellation there must be additional fields charged under the dark $U(1)$. However, we include only the lightest of such fields as the DM candidate, as the others can be made heavier such that the phenomenology is not affected, as they make a subdominant contribution to the relic density, as can be seen from section 4.3.

⁴It is also important to note that there exist relations between the axial-vector coupling size and the masses of the dark sector fields [58]. Therefore, for almost all mass choices of the dark sector fields, it is not possible to make the axial-vector coupling vanishingly small relative to the vector coupling without the vector coupling becoming non-perturbative. Thus, the axial-vector coupling is effectively never negligible and cannot be neglected even in limiting cases.

where the component fields of S and H are defined in the broken phase as $S \equiv \frac{1}{\sqrt{2}}(w + s + ia)$ and $H = \left\{ G^+, \frac{1}{\sqrt{2}}(v + h + iG^0) \right\}$ with G^+ , G^0 and a being the Goldstone bosons of W , Z and Z' respectively, while s and h are real scalars. The coupling g_f , which controls the interactions of the Z' with SM fermions, is dictated by the kinetic mixing; the explicit form can be found, e.g., in Ref. [102]. We assume that the scalar mixing parameter λ_{hs} is small, which implies that the SM Higgs is not significantly perturbed by the new physics. In this limit, the dark Higgs vev satisfies $w^2 = -\mu_s^2/\lambda_s$ and the various masses are:

$$m_{Z'} = g_\chi w, \quad (4.6a)$$

$$m_\chi = \frac{1}{\sqrt{2}} y_\chi w, \quad (4.6b)$$

$$m_s^2 \simeq -2\mu_s^2, \quad (4.6c)$$

$$m_h^2 \simeq -2\mu_h^2. \quad (4.6d)$$

Importantly, because both the DM and Z' masses are both proportional to the vev of the dark Higgs, their masses and couplings are not all independent parameters but instead are related as

$$y_\chi/g_\chi = \sqrt{2}m_\chi/m_{Z'}. \quad (4.7)$$

4.2 Cross Sections

The relevant annihilation processes for this scenario are shown in Tab. (1). The $\chi\bar{\chi} \rightarrow sZ'$ annihilation receives contributions from both s and t/u channel processes, while s -wave contributions to the $\chi\bar{\chi} \rightarrow Z'Z'$ process arise only from the t/u channel diagrams. (Note, however, that the contribution of the s -channel scalar exchange diagram to the annihilation to $Z'Z'$ is necessary to unitarize the cross section at high energy. Without this contribution, longitudinal Z'_L contributions would lead to unphysical high energy behavior of the p -wave term.) The s -wave contributions to the annihilation cross sections are given by

$$\langle\sigma v\rangle_{\chi\bar{\chi}\rightarrow Z'Z'} = \frac{g_\chi^4 (1 - \eta_{Z'})^{3/2} (16Q_V^4 \eta_{Z'} + 8Q_V^2 (4 - 3\eta_{Z'}) + \eta_{Z'})}{64\pi m_\chi^2 (\eta_{Z'} - 2)^2 \eta_{Z'}}, \quad (4.8)$$

and

$$\begin{aligned} \langle\sigma v\rangle_{\chi\bar{\chi}\rightarrow sZ'} &= \frac{g_\chi^4 \sqrt{(\eta_s - \eta_{Z'} - 4)^2 - 16\eta_{Z'}}}{1024\pi m_\chi^2 (\eta_{Z'} - 4)^2 \eta_{Z'}^2 (\eta_s + \eta_{Z'} - 4)^2} \times \\ &\left\{ (\eta_{Z'} - 4)^2 (\eta_s + \eta_{Z'} - 4)^2 ((\eta_s - \eta_{Z'} - 4)^2 - 16\eta_{Z'}) \right. \\ &+ 4Q_V^2 \eta_{Z'} \left[\eta_s^4 \eta_{Z'} - 16\eta_s^3 \eta_{Z'} - 2\eta_s^2 (\eta_{Z'}^3 - 44\eta_{Z'}^2 + 80\eta_{Z'} - 64) \right. \\ &\left. \left. + 64\eta_s (\eta_{Z'} - 4)^2 (\eta_{Z'} - 1) + (\eta_{Z'} - 4)^4 (\eta_{Z'} + 8) \right] \right\}, \quad (4.9) \end{aligned}$$

where $\eta_{s,Z'} = m_{s,Z'}^2/m_\chi^2$. As explained above, we have set $Q_S = 1 = 2Q_A$ without loss of generality, while Q_V is left as a free parameter. Also note that we have used Eq. (4.7) to replace the Yukawa coupling y_χ with the gauge coupling g_χ .

These annihilation cross sections are plotted in Fig. (1). We see that the $Z'Z'$ cross section becomes approximately independent of the DM mass when $m_\chi \gg m_{Z'}$, while the

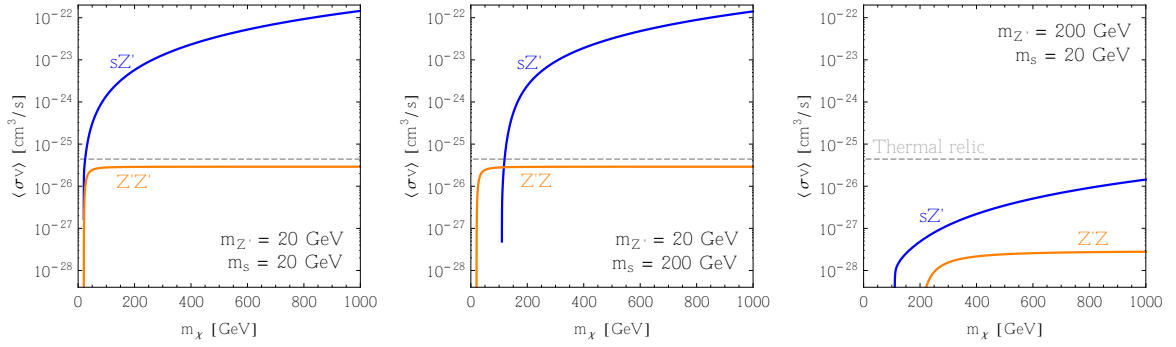


Figure 1. Relative cross sections for the two dominant s -wave annihilation processes in scenario II, $\chi\bar{\chi} \rightarrow sZ'$ (blue) and $\chi\bar{\chi} \rightarrow Z'Z'$ (orange), for example choices of the dark Higgs mass and the Z' mass, as labeled. This scenario requires $2Q_A = Q_S = 1$, and we have chosen $Q_V = 1/2$. The gauge coupling has been set to $g_\chi = 0.1$, but as all cross sections are directly proportional to g_χ^4 they can easily be scaled by adjusting this parameter. For reference, the approximate thermal relic cross section is shown as the gray dashed line.

sZ' cross section rises with m_χ . (This is to be contrasted with the behavior in cases III and IV, where all cross sections decline as m_χ is increased.) This is an interesting consequence of having both vector and axial-vector interactions present: For the $Z'Z'$ process, there is a $V - A$ interference which gives rise to longitudinal Z' domination in the $m_\chi^2 \gg m_{Z'}^2$ limit⁵. The sZ' process is also dominated by Z'_L contributions in this limit. This can be understood by appealing to the Goldstone boson equivalence theorem which, in the high energy limit, relates the amplitude for emission of a longitudinally polarized gauge boson (Z'_L) with that for the emission of the corresponding Goldstone boson (the pseudoscalar a). For the $\chi\bar{\chi} \rightarrow sZ'$ process, in addition to the transverse contributions we have $\chi\bar{\chi} \rightarrow sZ'_L$, which in the high energy limit is equivalent to $\chi\bar{\chi} \rightarrow sa$. As this scalar plus pseudoscalar final state is odd under parity, this is an s -wave process. For the $\chi\bar{\chi} \rightarrow Z'Z'$ process, if both Z'_L are replaced by their Goldstones we would have $\chi\bar{\chi} \rightarrow aa$, which is even under parity and thus p -wave. However, a combination of longitudinal and transverse modes are possible, $\chi\bar{\chi} \rightarrow Z'_L Z'_T$, which is equivalent to the s -wave process $\chi\bar{\chi} \rightarrow aZ'_T$ and thus dominates at high energy. Notice that the sZ' process, in addition to external Z'_L contributions, also receives contributions from the longitudinal Z' mode in the s -channel Z' propagator. This contribution leads to four powers of $m_{Z'}$ in the denominator of the sZ' cross section. In contrast, the $Z'Z'$ cross section receives Z'_L contributions only from a single final state Z' , and so has only two powers of $m_{Z'}$ in the denominator. The $Z'Z'$ process is thus sub-dominant to the sZ' process when both are kinematically allowed⁶.

4.3 Relic Density

An important requirement for a DM model is to produce the correct relic density. Note, however, that a full DM model is likely to have more dark sector fields than the simplified

⁵If Q_V were chosen to be zero, such that the Z' coupling were pure axial, there would be no $V - A$ interference and the s -wave part of the $Z'Z'$ cross section would *not* be enhanced by longitudinal Z' modes. This situation maps onto the Majorana DM case studied in Ref. [62].

⁶Note that because the Yukawa and gauge coupling constants are related via Eq. (4.7), it is not possible to change the relative size of the annihilation to $Z'Z'$ and sZ' by adjusting these parameters.

models considered here, which may impact the relic density determination. Nonetheless, we shall determine the relic density constraints for our simplified models, to serve as a guide to the viable regions of parameter space.

We use MICROMEAS 3 [103] to calculate the DM relic density, and compare with the recent determination by the Planck collaboration [104],

$$\Omega_\chi h^2 = 0.1196 \pm 0.0031. \quad (4.10)$$

For different Z' and dark Higgs mass, we scan the parameter space and find that the DM relic density can be saturated fairly easily. We show the relic contours in Fig. (2) as a function of m_χ and g_χ for fixed $m_{Z'}$ and m_s , and $Q_V = 1/2$. In each panel, the observed relic $\Omega_\chi h^2 = 0.1196$ is depicted by a black solid line, while red dot-dashed and blue dotted lines show contours for $\Omega_\chi h^2 = 0.01$ and 1.0 respectively. The central panel clearly shows the resonant enhancement of the annihilation to $Z'Z'$ through the s -channel scalar exchange, as a spike near $m_\chi \sim 100$ GeV. Other features of the relic contours in the middle and right panels are associated with the sZ' final state. The parameter regions shown in Fig. (2) all satisfy $\lambda_s < \sqrt{4\pi}$.

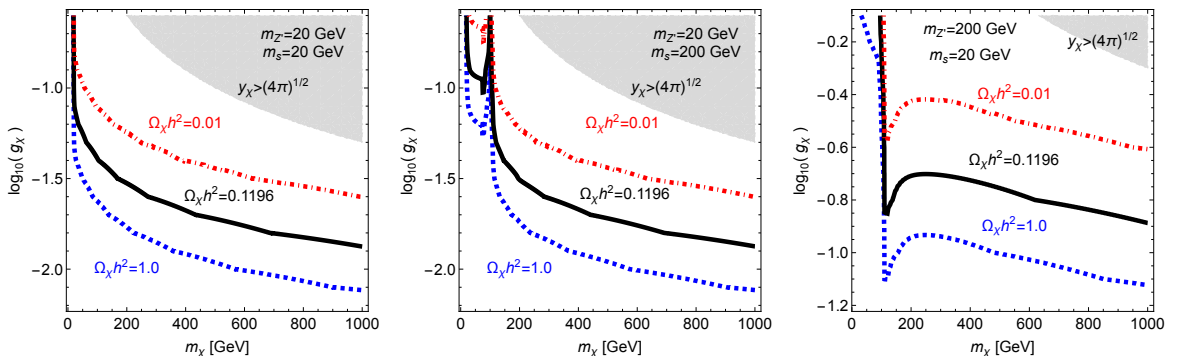


Figure 2. Dark matter relic density contours in scenario II, as a function of m_χ and g_χ , for various choices of the dark Higgs and Z' mass, as labeled. This scenario requires $2Q_A = Q_S = 1$, and we have chosen $Q_V = 1/2$. The red dot-dashed, the black solid and the blue dotted lines denote the contours for $\Omega_\chi h^2 = 0.01$, 0.1196 and 1.0 respectively. In the shaded region the Yukawa coupling y_χ is larger than $\sqrt{4\pi}$.

5 Scenario III: DM Mass from Dark Higgs Mechanism, Z' Mass from Stueckelberg Mechanism

Interaction type required: Pure Vector

We now consider a scenario where the mass of the χ and Z' arise from different mechanisms. Specifically, we assume the χ mass is due to a Higgs mechanism, while the Z' mass arises from the Stueckelberg mechanism. As a result only pure vector interactions of the χ and Z' are permitted. Here the dark $U(1)_\chi$ remains unbroken, and instead the dark Higgs must

break some other symmetry under which the DM is charged. This scenario divorces the Z' physics from the dark Higgs physics⁷.

5.1 Model

The most minimal Lagrangian for this setup is

$$\begin{aligned} \mathcal{L} = \mathcal{L}_{SM} &+ i\bar{\chi}(\not{\partial} + ig_\chi Q_V \not{Z}')\chi - \frac{y_\chi}{\sqrt{2}}\bar{\chi}\chi\phi \\ &+ \frac{1}{2}\partial_\mu\phi\partial^\mu\phi - \frac{1}{2}\mu_s^2\phi^2 - \frac{1}{4}\lambda_s\phi^4 - \frac{1}{2}\lambda_{hs}\phi^2(H^\dagger H) - \frac{\sin\epsilon}{2}Z'^{\mu\nu}B_{\mu\nu}, \end{aligned} \quad (5.1)$$

with the real scalar $\phi = w + s$, where w is the vev of ϕ and s is the dark Higgs. The vectorlike charge Q_V can be chosen freely. Again, the dark sector interacts with the visible sector in two ways: via kinetic mixing or Higgs mass mixing.

As the dark Higgs is responsible only for generating fermion masses, a real scalar is sufficient to accomplish this task. (The dark Higgs must break the $U(1)_\chi$ in all other scenarios we consider, which requires a complex scalar.) If we introduce a complex scalar instead, the extra degree of freedom will be a massless Goldstone boson and will contribute to the radiation energy density of the universe. If the Goldstones had the same temperature as the SM neutrinos, they would make a contribution equivalent to $N_{\text{eff}}^\nu = 4/7$, in marginal agreement with current experimental observations. However, their contribution to N_{eff}^ν would be suppressed if they decoupled early enough to not be heated by the annihilations of some SM species [105].

5.2 Cross Sections

As shown in Tab. (1), both the $Z'Z'$ and sZ' processes receive contributions only from the t/u channel diagrams, as the absence of a $Z'-s$ interaction eliminates the s -channel diagrams of scenario II. The s -wave contributions to the annihilation cross sections are given by

$$\langle\sigma v\rangle_{\chi\bar{\chi}\rightarrow Z'Z'} = \frac{g_\chi^4 Q_V^4 (1 - \eta_{Z'})^{3/2}}{4\pi m_\chi^2 (\eta_{Z'} - 2)^2} \quad (5.2)$$

and

$$\langle\sigma v\rangle_{\chi\bar{\chi}\rightarrow sZ'} = \frac{g_\chi^2 Q_V^2 y_\chi^2 \sqrt{(\eta_s - \eta_{Z'} - 4)^2 - 16\eta_{Z'}} \left((\eta_s - \eta_{Z'} - 4)^2 + 8\eta_{Z'} \right)}{64\pi m_\chi^2 (\eta_s + \eta_{Z'} - 4)^2}, \quad (5.3)$$

where $\eta_{s,Z'} = m_{s,Z'}^2/m_\chi^2$.

The relative size and behavior of these cross sections can be seen in Fig. (3). Given that the Z' obtains mass from the Stueckelberg mechanism, there are no contributions to the cross sections from longitudinal Z' modes. Therefore, all cross sections decrease with increasing DM mass. It is possible to dial the strength of one annihilation process relative to the other by adjusting the dark Yukawa coupling y_χ and the dark gauge coupling g_χ , which are independent parameters. (This freedom was not available in scenario II, where

⁷This situation has a SM analogue where χ is replaced by the electron and Z' is replaced by the photon: the electrons have vector couplings to the photon of an unbroken $U(1)_{\text{QED}}$; the electron mass comes from breaking the electroweak symmetry with the SM Higgs; the SM Higgs does not couple to the photon or contribute to the photon mass. The annihilation $\chi\bar{\chi} \rightarrow sZ'$ is then the analogue of $e^+e^- \rightarrow h\gamma$.

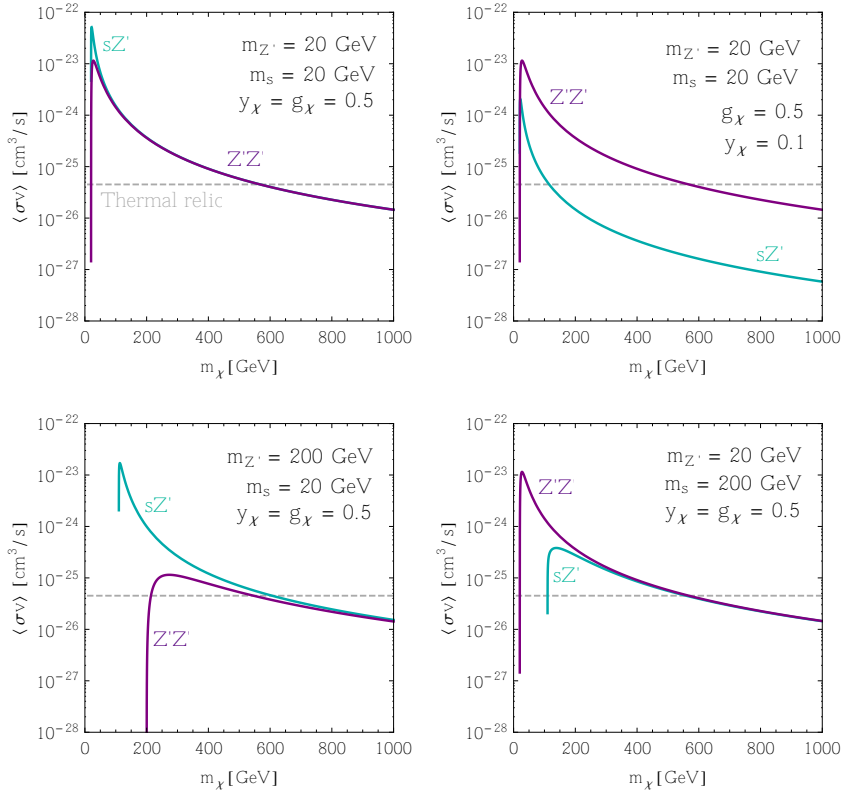


Figure 3. Cross section for the two dominant s -wave annihilation processes of scenario III, $\chi\bar{\chi} \rightarrow sZ'$ (blue) and $\chi\bar{\chi} \rightarrow Z'Z'$ (purple), for some example choices of the dark Higgs mass, the Z' mass, and the dark gauge and Yukawa couplings, as labeled. Here $Q_V = 1$. Notice, by comparing the top two panels, that either process can be chosen to dominate by varying the dark gauge coupling and the dark Yukawa coupling. The approximate thermal relic cross section is shown as the gray dashed line.

the couplings were related.) This is shown in the top two panels of Fig. (3). This also means that if $g_\chi \ll y_\chi$ then p -wave processes such as $\chi\bar{\chi} \rightarrow ss$ (which scale as y_χ^4) may have an important effect on the relic density, as the otherwise dominant $Z'Z'$ and sZ' processes (which scale as g_χ^4 and $g_\chi^2 y_\chi^2$ respectively) would be suppressed by the small gauge coupling. However, it is difficult to make the annihilation to ss dominate in the universe today, where the p -wave modes are suppressed by $v_\chi^2 \approx 10^{-6}$. To do so would require $g_\chi^2 \sim 10^{-6} y_\chi^2$ which, while possible, is a very tuned scenario that we shall not consider. The relevant diagrams for annihilation to ss are shown in Fig. (4).

5.3 Relic Density

In Fig. (5), we show the relic density contours as a function of DM mass m_χ and the dark gauge coupling g_χ for various values of the Z' mass, dark Higgs mass, $Q_V = 1$ and fixed ratios of y_χ/g_χ . The color codes for the contours are the same as in the previous scenario. The different choices of y_χ/g_χ are embodied in the thickness of the lines: thinner for $y_\chi/g_\chi = 1$ and thicker for $y_\chi/g_\chi = 5$. Obviously for the same g_χ , a larger y_χ/g_χ ratio results in a larger cross section for $\chi\bar{\chi} \rightarrow sZ'$ and thus a smaller relic density; a smaller g_χ is thus needed to obtain the same relic density, resulting in an overall downward shift of the contours. In this scenario,

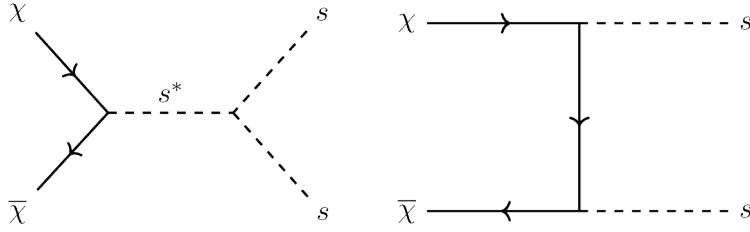


Figure 4. DM annihilation to two dark Higgs bosons, $\chi\bar{\chi} \rightarrow ss$. Despite being p -wave suppressed, these processes can make a non-negligible impact on the relic density at freeze-out, particularly if the gauge coupling is sufficiently small to suppress the s -wave processes.

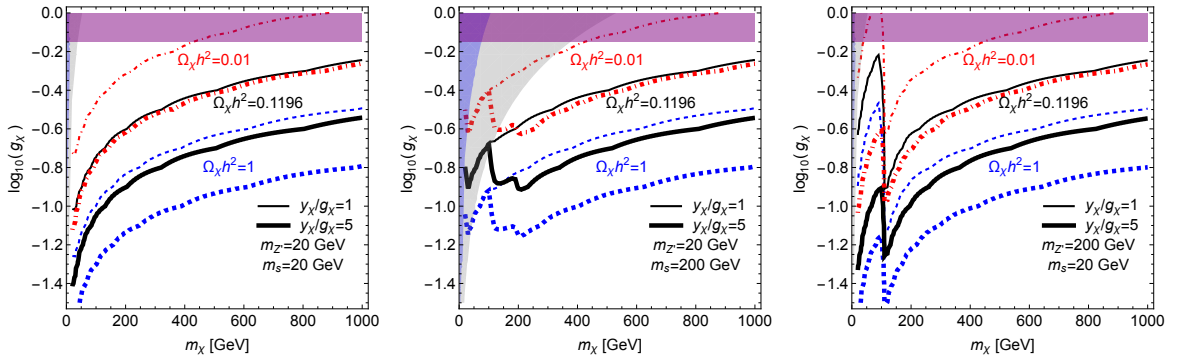


Figure 5. Relic density contours for scenario III, as a function of m_χ and g_χ , for various choices of the dark Higgs and Z' mass and ratio of couplings constants, as labeled. The thin (thick) red dot-dashed, solid black and dotted blue lines denote $\Omega h^2 = 0.01, 0.1196$ and 1 , respectively, for $y_\chi/g_\chi = 1$ (5). In the light purple shaded regions, the Yukawa coupling y_χ is larger than $\sqrt{4\pi}$ for $y_\chi/g_\chi = 5$; it is always perturbative in the parameter space shown when $y_\chi/g_\chi = 1$. The region shaded blue (gray) on the left side of each panel shows the perturbativity bound for λ_s with $y_\chi/g_\chi = 1$ (5).

the quartic coupling λ_s can be expressed as $\lambda_s \simeq y_\chi^2 m_s^2 / (4m_\chi^2)$. The perturbativity bounds for λ_s are shown by the shaded gray regions, while the parameter space where $y_\chi > \sqrt{4\pi}$ ($y_\chi/g_\chi = 5$ only) is shown as the light purple region.

The dips in Fig. (5) correspond to kinematic opening of various channels when $2m_\chi > m_1 + m_2$ with $m_{1,2}$ being the masses of the annihilation product. For $2m_\chi < m_1 + m_2$, the annihilation of DM through these channels will be exponentially suppressed. So in the left panel, where $m_{Z'} = m_s = 20$ GeV, all three channels, sZ' , $Z'Z'$ and ss , are open at the same time and no dips occur beyond this mass. For the middle and right panels of Fig. (5), there is a dip at $m_\chi \simeq 110$ GeV corresponding to the sZ' channel. In the middle panel, the ss channel begins to contribute around $m_\chi \simeq 200$ GeV; the effect is more pronounced for larger y_χ , leading to a prominent dip for $y_\chi/g_\chi = 5$ but not for $y_\chi/g_\chi = 1$. In the right panel, however, there is no dip around 200 GeV for the $Z'Z'$ channel, since the $Z'Z'$ cross section is always subdominant to the sZ' cross section for the couplings chosen.

6 Scenario IV: Bare DM Mass, Z' Mass from Dark Higgs Mechanism

Interaction type required: Pure Vector

An alternative scenario in which the mass of the DM and Z' arise from different mechanisms, is to have a bare mass for the χ and use a dark Higgs mechanism to provide mass for the Z' . In this scenario, again, only pure vector interactions of the χ and Z' are permitted.

6.1 Model

In this scenario, the most minimal gauge invariant Lagrangian is

$$\begin{aligned} \mathcal{L} = & \mathcal{L}_{SM} + i\bar{\chi}(\not{\partial} + ig_\chi Q_V \not{Z}')\chi - \frac{\sin\epsilon}{2}Z'^{\mu\nu}B_{\mu\nu} - m_\chi\bar{\chi}\chi \\ & + [(\partial^\mu + ig_\chi Q_S Z'^\mu)S]^\dagger [(\partial_\mu + ig_\chi Q_S Z'_\mu)S] - \mu_s^2 S^\dagger S - \lambda_s(S^\dagger S)^2 - \lambda_{hs}(S^\dagger S)(H^\dagger H). \end{aligned} \quad (6.1)$$

The vectorlike charge Q_V and dark Higgs charge Q_S under the dark $U(1)_\chi$ can be chosen freely. Again the dark sector interacts with the visible sector in two ways: via kinetic mixing or Higgs mass mixing.

6.2 Cross Sections

As shown in Tab. (1), the annihilation to sZ' proceeds only via the s -channel diagram, as the DM does not interact directly with the dark Higgs. The annihilation to $Z'Z'$ proceeds via the t/u and channel diagrams. The s -wave contributions to these annihilation cross sections are given by

$$\langle\sigma v\rangle_{\chi\bar{\chi}\rightarrow Z'Z'} = \frac{g_\chi^4 Q_V^4 (1 - \eta_{Z'})^{3/2}}{4\pi m_\chi^2 (\eta_{Z'} - 2)^2} \quad (6.2)$$

and

$$\langle\sigma v\rangle_{\chi\bar{\chi}\rightarrow sZ'} = \frac{g_\chi^4 Q_V^2 Q_S^2 \sqrt{(\eta_s - \eta_{Z'} - 4)^2 - 16\eta_{Z'}} \left((\eta_s - \eta_{Z'} - 4)^2 + 32\eta_{Z'} \right)}{256\pi m_\chi^2 (\eta_{Z'} - 4)^2}, \quad (6.3)$$

where $\eta_{s,Z'} = m_{s,Z'}^2/m_\chi^2$. The behavior of these cross sections is depicted in Fig. (6). We see that the shapes of the sZ' and $Z'Z'$ cross sections are similar, as both fall off with DM mass as $1/m_\chi^2$. There is no production of longitudinal Z'_L modes in the high energy limit, which is consistent with the fact that the DM does not interact with Goldstone modes, given the absence of a DM-Higgs coupling. Because Q_V and Q_S are independent, the relative size of the $Z'Z'$ and sZ' processes can again be scaled relative to each other by appropriate choices of these charges.

6.3 Relic Density

We plot the relic density contours for this scenario in Fig. (7). As the dark Higgs is responsible for the Z' mass, the quartic coupling may be expressed as $\lambda_s \simeq g_\chi^2 m_s^2 / (2m_{Z'}^2)$. Parameters excluded by the perturbativity bound on λ_s are shaded gray; this bound is relevant only for the middle panel of Fig. (7), where the ratio of $m_s/m_{Z'}$ is larger. Because there is no direct coupling of the scalar to the DM, there is no annihilation to ss . As a result, the features of the relic density contours are generally simpler than in the previous scenario. For the chosen

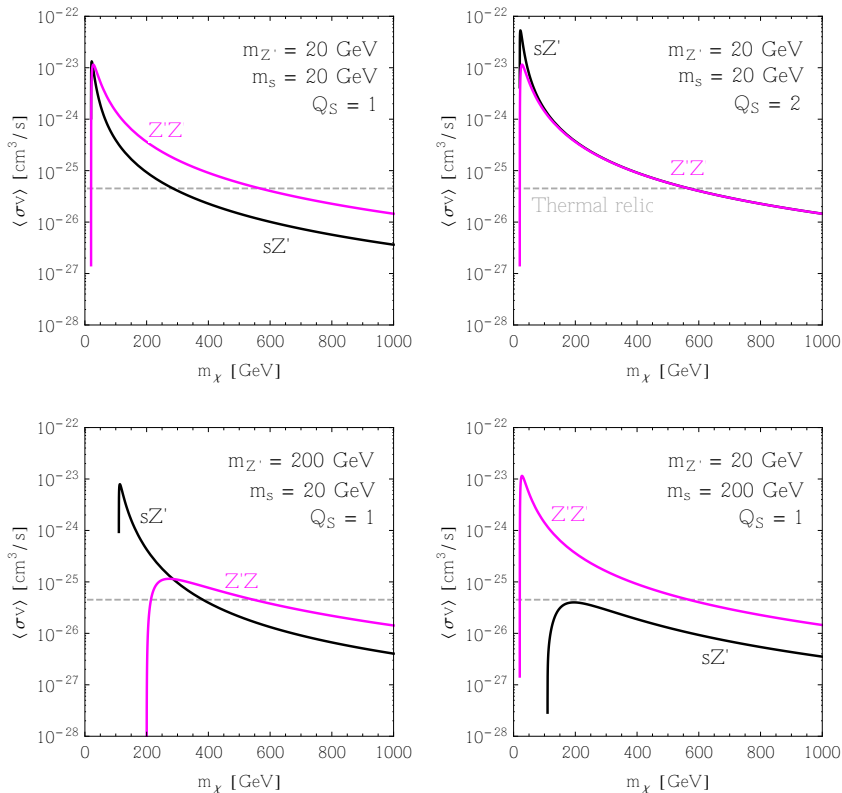


Figure 6. Relative cross section for the two dominant s -wave annihilation processes in scenario IV, $\chi\bar{\chi} \rightarrow sZ'$ (black) and $\chi\bar{\chi} \rightarrow Z'Z'$ (magenta), for some example parameter choices for the dark Higgs mass and Z' mass, as labeled. Here $Q_V = 1$. Example dark charges $Q_S = 1, 2$ are shown, which demonstrate how either process can be made to dominate, or both can be made comparable, if kinematically allowed. For all plots the gauge coupling is set to $g_\chi = 0.5$. As all cross sections are directly proportional to g_χ^4 they can easily be scaled by adjusting this parameter. The approximate thermal relic cross section is shown as the gray dashed line.

values of $Q_{V,S}$, the annihilation to sZ' is subdominant to the $Z'Z'$ process when both are kinematically allowed. This leads to a dip in the contours of the right panel at $m_\chi \simeq m_{Z'}$, where the $Z'Z'$ modes becomes allowed, but not in the left and center panels where the $Z'Z'$ mode always plays the dominant role.

7 Indirect Detection Phenomenology

We now determine indirect detection constraints on the dominant annihilation modes for the scenarios discussed, $\chi\bar{\chi} \rightarrow Z'Z'$ and $\chi\bar{\chi} \rightarrow sZ'$. The Z' and s produced in these annihilations decay to SM particles, and subsequent hadronization/decay of these SM states leads to gamma-ray and other fluxes that we may compare with observational limits.

We generate our gamma-ray spectra as per the method outlined in Ref. [62], where a more detailed description can be found. The kinetic mixing of the Z' with the SM hypercharge

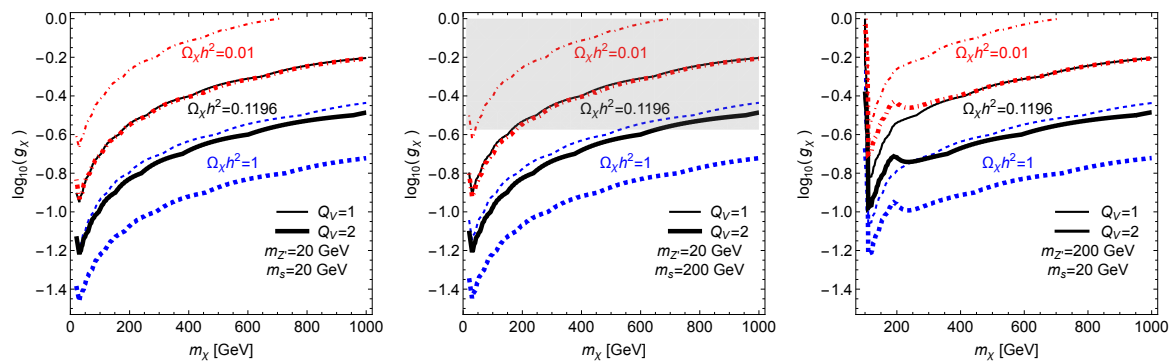


Figure 7. Dark matter relic density contours for scenario IV as a function of m_χ and g_χ , for various choices of m_s , $m_{Z'}$ and Q_V , as labeled. The thin (thick) red dot-dashed, solid black and dotted blue lines denote $\Omega_\chi h^2 = 0.01, 0.1196$ and 1 , respectively, for $Q_V = 1$ (2). We have taken $Q_S = 1$. For the chosen values of $Q_{V,S}$, the sZ' contribution is subdominant to that from $Z'Z'$ when both are kinematically allowed, which accounts for the features of the curves. The light gray shaded region at the top of the middle panel shows the parameter space excluded by perturbativity bound for λ_s .

boson permits the decay $Z' \rightarrow f\bar{f}$, with a partial width given by

$$\Gamma(Z' \rightarrow f\bar{f}) = \frac{m_{Z'} N_c}{12\pi} \sqrt{1 - \frac{4m_f^2}{m_{Z'}^2}} \left[g_{f,V}^2 \left(1 + \frac{2m_f^2}{m_{Z'}^2} \right) + g_{f,A}^2 \left(1 - \frac{4m_f^2}{m_{Z'}^2} \right) \right], \quad (7.1)$$

where N_c is a color factor, relevant for hadronic decays. The $g_{f,V}$ (vector) and $g_{f,A}$ (axial-vector) structure of the $Z'-f$ couplings are inherited from the kinetic mixing [102]. The total decay width for the Z' is then simply given by the sum over all the final state fermions, $\Gamma_{Z'} = \sum_f \Gamma(Z' \rightarrow f\bar{f})$. The dark Higgs decays to the SM due to mass mixing with the SM Higgs, and so it decays preferentially to heavier particles. The dark Higgs is also permitted to decay to pairs of Z' . In order to take into account loop decays and higher order corrections, we calculate the dark Higgs decay widths numerically with the FORTRAN package HDECAY [106].

The spectra generated are then compared to the strongest indirect detection limits available for our processes⁸: the Fermi-LAT Pass 8 data on dwarf spheroidal galaxies (dSphs) of the Milky Way [36]. To find the limit on the cross section from dSphs, we use the maximal likelihood method to compare our spectra against those for the dSphs publicly provided by Fermi-LAT in the Pass 8 data, with the J factor taken to be a nuisance parameter as per Ref. [36]. We take spectra from 15 dSphs: Bootes I, Canes Venatici II, Carina, Coma Berenices, Draco, Fornax, Hercules, Leo II, Leo IV, Sculptor, Segue 1, Sextans, Ursa Major II, Ursa Minor, and Willman 1. The 95% C.L. limits on the annihilation cross section are shown Fig. (8), for various dark Higgs and Z' masses, for both sZ' and $Z'Z'$ processes.

The limits we show are independently set on either the $\chi\bar{\chi} \rightarrow sZ'$ process or the $\chi\bar{\chi} \rightarrow Z'Z'$ process. They can then be applied to any of the scenarios we study in this paper, assuming that one of the modes dominates. Indeed, they can also be applied to any model that features annihilations to a sZ' or $Z'Z'$ final state, provided the Z' and s communicate with the SM via kinetic or Higgs mass mixing respectively, as the cross section limits depend

⁸We also include the approximate limit from AMS-02 at low DM masses, adapted from [85]. This approximate limit is only applicable if the sum of the final state mediators is less than about 70 GeV.

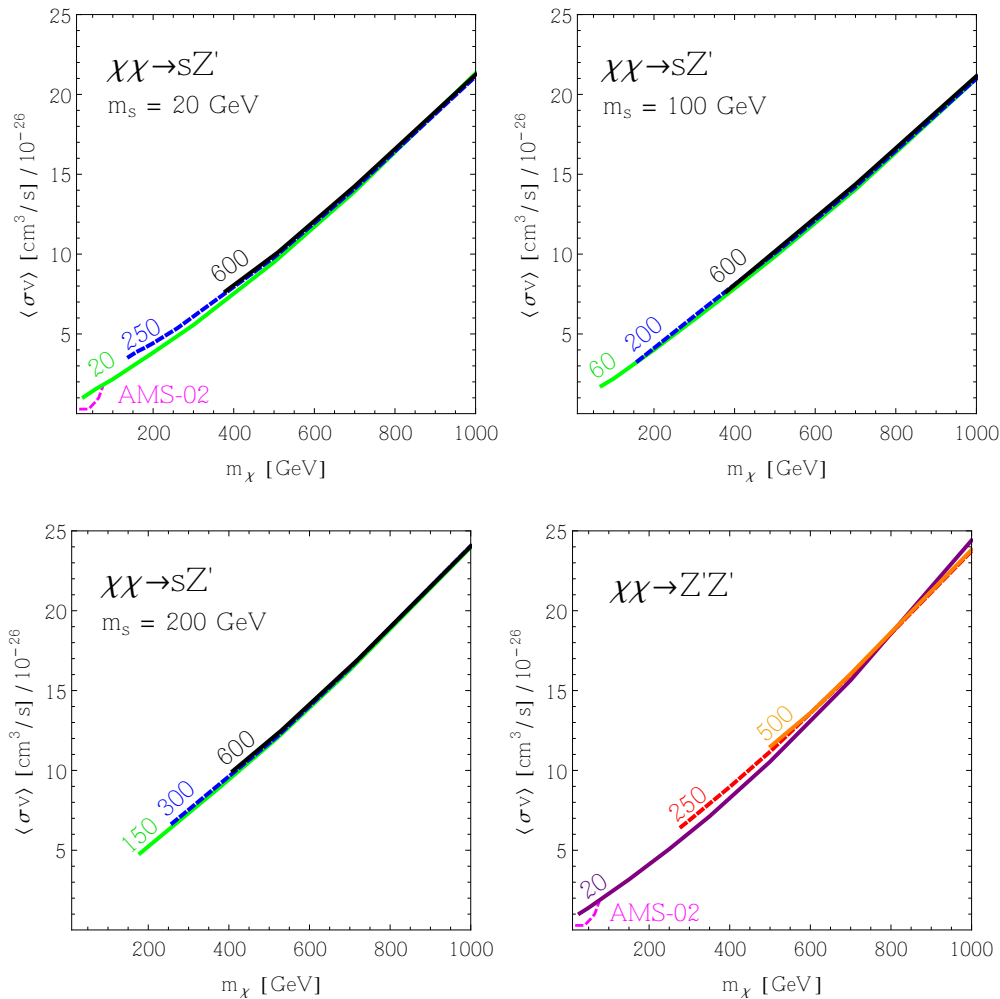


Figure 8. 95% confidence limits (C.L.) on the annihilation cross section from Fermi Pass 8 data on 15 dwarf spheroidal galaxies. Limits on the sZ' process are shown for dark Higgs masses of 20, 100 and 200 GeV, for various Z' masses as labeled in the plots. Z' masses stated are in GeV. Limits on the $Z'Z'$ process are shown for Z' masses of 20, 250 and 500 GeV. The approximate limit from AMS-02 is shown as a dashed magenta line, and is only applicable if the sum of the final state mediators is less than about 70 GeV. Intermediate mediator mass limits can be simply obtained from interpolation of these plots. All these plots can be applicable to any of the scenarios outlined in this paper: the appropriate limit of sZ' or $Z'Z'$ will depend on the specific choices of the couplings, masses and for which process is kinematically allowed.

only on the gamma-ray spectral shape that characterizes a given annihilation mode. From Fig. (8) it is clear that the limit on the cross section does not vary greatly with the mediator mass provided it is kinematically allowed; it is instead the DM mass with which the energy of final state photons and thus cross section limits is tightly correlated.

The thermal relic cross section required to reproduce the correct relic density for non-self conjugate DM is approximately $\langle\sigma v\rangle \approx 4.4 \times 10^{-26}$ cm³/s [107], which excludes the low DM mass region where the Fermi limits surpass this sensitivity. However, this statement assumes that the s -wave contributions to the annihilation cross section dominate both at freeze-out

and in the universe today. In fact in some cases, such as scenario III, the p -wave processes can make a non-negligible contribution at freeze-out. This means that the relic density constraint could be satisfied, yet the cross section in the universe today suppressed, escaping indirect detection bounds even for low DM mass.

8 Discussion and Summary

We have surveyed a spectrum of phenomenologically distinct two-mediator DM models, containing both a dark vector and dark scalar, where gauge invariance is respected and the mass terms for the dark sector fields are introduced in a self-consistent way. These two-mediator DM models correctly capture important phenomenology which is missing in the single mediator approach. Specifically, we modified the usual simplified model setup to incorporate mass generation for the DM candidate and vector mediator, by using combinations of bare mass terms, Higgs mechanisms and Stueckelberg mechanisms. We found that the DM interaction types and annihilation processes, and hence both the relic density and indirect detection constraints, are strongly dictated by the mass generation mechanism we choose for the dark sector particles:

- Unless the DM and Z' masses both receive contributions from the vev of the same dark Higgs field, pure vector couplings of the spin-1 mediator and DM are required, as discussed in scenarios III and IV. In these scenarios DM annihilates to both sZ' and $Z'Z'$, with the relative rates to these final states controlled by independent coupling constants. Moreover, in the high energy limit, only the Z'_T polarization is produced by these annihilations.
- However, if a dark Higgs mechanism gives mass to all the dark sector fields, as per scenario II, the axial-vector coupling between the spin-1 mediator and DM must be non-zero. In this scenario, the sZ' and $Z'Z'$ DM annihilation channels are intrinsically linked. Furthermore, production of the Z'_L polarization enhances the annihilation to sZ' . If both the vector and axial-vector couplings are non-zero, the annihilation to $Z'Z'$ is also enhanced by Z'_L (via the $V - A$ interference) though it remains subdominant to the sZ' mode when both are kinematically allowed.

One may imagine generalizations of scenarios III and IV in which the Z' and χ masses arise from *two different* Higgs mechanisms. Indeed, we would recover scenario III (Stueckelberg Z' mass) in the limit that the Higgs responsible for the Z' mass is taken to infinity. Likewise, we would recover scenario IV (bare χ mass) in the limit that the Higgs responsible for the χ mass is taken very large. In these generalizations, the χ - Z' coupling remains of pure vector form. Axial couplings always imply that a Higgs which Yukawa couples to the χ must carry $U(1)_\chi$ charge, and hence its vev also contributes to the Z' mass, as in scenario II. Such two-scalar models would lead to additional complexity via mixing in the scalar sector, but would not introduce any qualitatively new Z' physics.

Our results are not captured by the single mediator approach, where the mass generation mechanism is left unspecified and constraints on the coupling types are not usually applied. This means that by continuing to use simplified models with a single spin-1 mediator, (i) we are at best only testing a very specific subset of the possibilities: Dirac DM with a bare mass and pure vector couplings to a Z' with a Stueckelberg derived mass (i.e. scenario I) or (ii) at worst, experimental constraints may not be meaningful because the models have

been oversimplified. Option (i) is not particularly appealing in that it does not cover well motivated possibilities such as Higgs mass generation (which, after all, is a mechanism we know is realized by nature) or Majorana DM. The remaining option, (ii), is far from desirable.

Acknowledgements

This work was supported in part by the Australian Research Council. RKL thanks John Beacom and the Center for Cosmology and AstroParticle Physics (CCAPP) at Ohio State University for their hospitality and support during her visit, where part of this work was completed. Feynman diagrams are drawn using TIKZ-FEYNMAN [108].

Appendix

A Cross Sections

In the scenarios discussed in this paper, the charges were fixed to particular values either to satisfy gauge invariance, or to demonstrate the phenomenology. The full cross sections with explicit $Q_{A,V}$ and Q_S dependence are listed in this appendix for reference.

The full s -wave cross section for $\chi\bar{\chi} \rightarrow Z'Z'$ is

$$\langle\sigma v\rangle_{\chi\bar{\chi}\rightarrow Z'Z'} = \frac{g_\chi^4 (1 - \eta_{Z'})^{3/2} (2Q_A^2 Q_V^2 (4 - 3\eta_{Z'}) + Q_A^4 \eta_{Z'} + Q_V^4 \eta_{Z'})}{4\pi m_\chi^2 (\eta_{Z'} - 2)^2 \eta_{Z'}}. \quad (\text{A.1})$$

This expression gives the s -wave contribution to the $\chi\bar{\chi} \rightarrow Z'Z'$ cross section for *all* cases, as only the t/u channel diagrams contribute. (Scalar-mediator contributions only enter at the p -wave level.) We see that if either Q_A or Q_V is zero, the cross section scales as $1/m_\chi^2$ in the limit that $\eta_{Z'} = m_{Z'}^2/m_\chi^2 \ll 1$, and is dominated by Z'_T contributions only. In the case that both Q_A and Q_V are non-zero, the cross section instead scales as $1/m_{Z'}^2$ in the $\eta_{Z'} \ll 1$ limit, which arises due to the Z'_L modes. Note however, that no violation of unitarity will occur – the Z' mass cannot be made arbitrarily large while satisfying the constraint Eq. (4.7) and restricting all couplings to perturbative values. This $Z'Z'$ cross section matches that in Refs. [109, 110].

The full s -wave cross section for $\chi\bar{\chi} \rightarrow sZ'$ is

$$\begin{aligned} \langle\sigma v\rangle_{\chi\bar{\chi}\rightarrow sZ'} &= \frac{g_\chi^2 \sqrt{(\eta_s - \eta_{Z'} - 4)^2 - 16\eta_{Z'}}}{256\pi m_\chi^2 (\eta_{Z'} - 4)^2 \eta_{Z'}^2 (\eta_s + \eta_{Z'} - 4)^2} \times \\ &\left\{ g_\chi^2 Q_S^2 (\eta_s + \eta_{Z'} - 4)^2 \left[Q_A^2 (\eta_{Z'} - 4)^2 \left((\eta_s - \eta_{Z'} - 4)^2 - 16\eta_{Z'} \right) \right. \right. \\ &\quad \left. \left. + Q_V^2 \eta_{Z'}^2 \left((\eta_s - \eta_{Z'} - 4)^2 + 32\eta_{Z'} \right) \right] \right. \\ &\quad \left. + 24\sqrt{2} g_\chi Q_S Q_V^2 y_\chi (\eta_{Z'} - 4) \eta_{Z'}^{5/2} (\eta_s^2 - 8\eta_s - \eta_{Z'}^2 + 16) \right. \\ &\quad \left. + 4Q_V^2 y_\chi^2 (\eta_{Z'} - 4)^2 \eta_{Z'}^2 \left((\eta_s - \eta_{Z'} - 4)^2 + 8\eta_{Z'} \right) \right\}. \quad (\text{A.2}) \end{aligned}$$

Taking $2Q_A = Q_S = 1$ and using the relation of the Yukawa and gauge coupling in Eq. (4.7) recovers the cross sections for scenario II, $Q_A = Q_S = 0$ recovers the cross sections for scenario III, and $Q_A, y_\chi = 0$ gives the cross sections for scenario IV.

It is still important to note however that the values for the charges cannot be chosen freely and should obey the constraints discussed in this paper.

References

- [1] L. Bergstrom, *Nonbaryonic dark matter: Observational evidence and detection methods*, *Rept. Prog. Phys.* **63** (2000) 793, [[hep-ph/0002126](#)].
- [2] G. Bertone, D. Hooper, and J. Silk, *Particle dark matter: Evidence, candidates and constraints*, *Phys.Rept.* **405** (2005) 279–390, [[hep-ph/0404175](#)].
- [3] **LUX** Collaboration, D. S. Akerib et al., *First results from the LUX dark matter experiment at the Sanford Underground Research Facility*, *Phys. Rev. Lett.* **112** (2014) 091303, [[arXiv:1310.8214](#)].
- [4] **LUX** Collaboration, D. S. Akerib et al., *Improved Limits on Scattering of Weakly Interacting Massive Particles from Reanalysis of 2013 LUX Data*, *Phys. Rev. Lett.* **116** (2016), no. 16 161301, [[arXiv:1512.03506](#)].
- [5] **PandaX-II** Collaboration, A. Tan et al., *Dark Matter Results from First 98.7-day Data of PandaX-II Experiment*, [arXiv:1607.07400](#).
- [6] **ATLAS** Collaboration, M. Aaboud et al., *Search for new phenomena in final states with an energetic jet and large missing transverse momentum in pp collisions at $\sqrt{s} = 13$ TeV using the ATLAS detector*, *Phys. Rev.* **D94** (2016), no. 3 032005, [[arXiv:1604.07773](#)].
- [7] **ATLAS** Collaboration, M. Aaboud et al., *Search for new phenomena in events with a photon and missing transverse momentum in pp collisions at $\sqrt{s} = 13$ TeV with the ATLAS detector*, *JHEP* **06** (2016) 059, [[arXiv:1604.01306](#)].
- [8] **ATLAS** Collaboration, M. Aaboud et al., *Search for dark matter produced in association with a hadronically decaying vector boson in pp collisions at $\sqrt{s}=13$ TeV with the ATLAS detector*, [arXiv:1608.02372](#).
- [9] **ATLAS** Collaboration, *Search for Dark Matter production associated with bottom quarks with 13.3 fb^{-1} of pp collisions at $\sqrt{s} = 13$ TeV with the ATLAS detector at the LHC*, . ATLAS-CONF-2016-086.
- [10] **ATLAS** Collaboration, *Search for Dark Matter in association with a Higgs boson decaying to b-quarks in pp collisions at $\sqrt{s} = 13$ TeV with the ATLAS detector*, . ATLAS-CONF-2016-019.
- [11] **CMS** Collaboration, C. Collaboration, *Search for new physics in a boosted hadronic monotop final state using 12.9 fb^{-1} of $\sqrt{s} = 13$ TeV data*, . CMS-PAS-EXO-16-040.
- [12] **CMS** Collaboration, C. Collaboration, *Search for dark matter and graviton produced in association with a photon in pp collisions at $\sqrt{s} = 13$ TeV*, . CMS-PAS-EXO-16-039.
- [13] **CMS** Collaboration, C. Collaboration, *Search for dark matter in $Z + E_{\text{T}}^{\text{miss}}$ events using 12.9 fb^{-1} of 2016 data*, . CMS-PAS-EXO-16-038.
- [14] **CMS** Collaboration, C. Collaboration, *Search for dark matter in final states with an energetic jet, or a hadronically decaying W or Z boson using 12.9 fb^{-1} of data at $\sqrt{s} = 13$ TeV*, . CMS-PAS-EXO-16-037.
- [15] **CMS** Collaboration, C. Collaboration, *Search for dark matter in association with a Higgs boson decaying into a pair of bottom quarks at $\sqrt{s} = 13$ TeV with the CMS detector*, . CMS-PAS-EXO-16-012.
- [16] **CMS** Collaboration, C. Collaboration, *Search for Dark Matter Produced in Association with a Higgs Boson Decaying to Two Photons*, . CMS-PAS-EXO-16-011.
- [17] **CMS** Collaboration, C. Collaboration, *Search for dark matter in association with a top quark pair at $\sqrt{s}=13$ TeV*, . CMS-PAS-EXO-16-005.
- [18] **CMS** Collaboration, C. Collaboration, *Search for Dark Matter produced in association with bottom quarks*, . CMS-PAS-B2G-15-007.

- [19] L. M. Carpenter, A. Nelson, C. Shimmin, T. M. P. Tait, and D. Whiteson, *Collider searches for dark matter in events with a Z boson and missing energy*, *Phys. Rev.* **D87** (2013), no. 7 074005, [[arXiv:1212.3352](#)].
- [20] L. Carpenter, A. DiFranzo, M. Mulhearn, C. Shimmin, S. Tulin, and D. Whiteson, *Mono-Higgs-boson: A new collider probe of dark matter*, *Phys. Rev.* **D89** (2014), no. 7 075017, [[arXiv:1312.2592](#)].
- [21] A. A. Petrov and W. Shepherd, *Searching for dark matter at LHC with Mono-Higgs production*, *Phys. Lett.* **B730** (2014) 178–183, [[arXiv:1311.1511](#)].
- [22] N. F. Bell, J. B. Dent, A. J. Galea, T. D. Jacques, L. M. Krauss, and T. J. Weiler, *Searching for Dark Matter at the LHC with a Mono-Z*, *Phys. Rev.* **D86** (2012) 096011, [[arXiv:1209.0231](#)].
- [23] N. F. Bell, Y. Cai, and R. K. Leane, *Mono-W Dark Matter Signals at the LHC: Simplified Model Analysis*, *JCAP* **1601** (2016), no. 01 051, [[arXiv:1512.00476](#)].
- [24] A. Birkedal, K. Matchev, and M. Perelstein, *Dark matter at colliders: A Model independent approach*, *Phys. Rev.* **D70** (2004) 077701, [[hep-ph/0403004](#)].
- [25] Y. Gershtein, F. Petriello, S. Quackenbush, and K. M. Zurek, *Discovering hidden sectors with mono-photon Z' o searches*, *Phys. Rev.* **D78** (2008) 095002, [[arXiv:0809.2849](#)].
- [26] J. Goodman, M. Ibe, A. Rajaraman, W. Shepherd, T. M. P. Tait, and H.-B. Yu, *Constraints on Dark Matter from Colliders*, *Phys. Rev.* **D82** (2010) 116010, [[arXiv:1008.1783](#)].
- [27] A. Crivellin, U. Haisch, and A. Hibbs, *LHC constraints on gauge boson couplings to dark matter*, *Phys. Rev.* **D91** (2015) 074028, [[arXiv:1501.00907](#)].
- [28] F. J. Petriello, S. Quackenbush, and K. M. Zurek, *The Invisible Z' at the CERN LHC*, *Phys. Rev.* **D77** (2008) 115020, [[arXiv:0803.4005](#)].
- [29] A. Berlin, T. Lin, and L.-T. Wang, *Mono-Higgs Detection of Dark Matter at the LHC*, *JHEP* **06** (2014) 078, [[arXiv:1402.7074](#)].
- [30] T. Lin, E. W. Kolb, and L.-T. Wang, *Probing dark matter couplings to top and bottom quarks at the LHC*, *Phys. Rev.* **D88** (2013), no. 6 063510, [[arXiv:1303.6638](#)].
- [31] P. J. Fox, R. Harnik, J. Kopp, and Y. Tsai, *Missing Energy Signatures of Dark Matter at the LHC*, *Phys. Rev.* **D85** (2012) 056011, [[arXiv:1109.4398](#)].
- [32] Y. Bai, J. Bourbeau, and T. Lin, *Dark matter searches with a mono-Z jet*, *JHEP* **06** (2015) 205, [[arXiv:1504.01395](#)].
- [33] M. Autran, K. Bauer, T. Lin, and D. Whiteson, *Searches for dark matter in events with a resonance and missing transverse energy*, *Phys. Rev.* **D92** (2015), no. 3 035007, [[arXiv:1504.01386](#)].
- [34] A. Gupta, R. Primulando, and P. Saraswat, *A New Probe of Dark Sector Dynamics at the LHC*, *JHEP* **09** (2015) 079, [[arXiv:1504.01385](#)].
- [35] K. Ghorbani and L. Khalkhali, *Mono-Higgs signature in fermionic dark matter model*, [[arXiv:1608.04559](#)].
- [36] **Fermi-LAT** Collaboration, M. Ackermann et al., *Searching for Dark Matter Annihilation from Milky Way Dwarf Spheroidal Galaxies with Six Years of Fermi Large Area Telescope Data*, *Phys. Rev. Lett.* **115** (2015), no. 23 231301, [[arXiv:1503.02641](#)].
- [37] J. Abdallah, A. Ashkenazi, A. Boveia, G. Busoni, A. De Simone, et al., *Simplified Models for Dark Matter and Missing Energy Searches at the LHC*, [[arXiv:1409.2893](#)].
- [38] M. R. Buckley, D. Feld, and D. Goncalves, *Scalar Simplified Models for Dark Matter*, *Phys.Rev.* **D91** (2015) 015017, [[arXiv:1410.6497](#)].

- [39] **LHC New Physics Working Group** Collaboration, D. Alves et al., *Simplified Models for LHC New Physics Searches*, *J.Phys.* **G39** (2012) 105005, [[arXiv:1105.2838](#)].
- [40] J. Alwall, P. Schuster, and N. Toro, *Simplified Models for a First Characterization of New Physics at the LHC*, *Phys.Rev.* **D79** (2009) 075020, [[arXiv:0810.3921](#)].
- [41] J. Abdallah et al., *Simplified Models for Dark Matter Searches at the LHC*, *Phys. Dark Univ.* **9-10** (2015) 8–23, [[arXiv:1506.03116](#)].
- [42] D. Abercrombie et al., *Dark Matter Benchmark Models for Early LHC Run-2 Searches: Report of the ATLAS/CMS Dark Matter Forum*, [arXiv:1507.00966](#).
- [43] A. De Simone and T. Jacques, *Simplified Models vs. Effective Field Theory Approaches in Dark Matter Searches*, [arXiv:1603.08002](#).
- [44] T. Jacques, A. Katz, E. Morgante, D. Racco, M. Rameez, and A. Riotto, *Complementarity of DM Searches in a Consistent Simplified Model: the Case of Z'* , [arXiv:1605.06513](#).
- [45] J. Goodman, M. Ibe, A. Rajaraman, W. Shepherd, T. M. P. Tait, and H.-B. Yu, *Constraints on Light Majorana dark Matter from Colliders*, *Phys. Lett.* **B695** (2011) 185–188, [[arXiv:1005.1286](#)].
- [46] M. Duch, B. Grzadkowski, and J. Wudka, *Classification of effective operators for interactions between the Standard Model and dark matter*, [arXiv:1412.0520](#).
- [47] I. M. Shoemaker and L. Vecchi, *Unitarity and Monojet Bounds on Models for DAMA, CoGeNT, and CRESST-II*, *Phys. Rev.* **D86** (2012) 015023, [[arXiv:1112.5457](#)].
- [48] P. J. Fox, R. Harnik, R. Primulando, and C.-T. Yu, *Taking a Razor to Dark Matter Parameter Space at the LHC*, *Phys. Rev.* **D86** (2012) 015010, [[arXiv:1203.1662](#)].
- [49] G. Busoni, A. De Simone, E. Morgante, and A. Riotto, *On the Validity of the Effective Field Theory for Dark Matter Searches at the LHC*, *Phys. Lett.* **B728** (2014) 412–421, [[arXiv:1307.2253](#)].
- [50] O. Buchmuller, M. J. Dolan, and C. McCabe, *Beyond Effective Field Theory for Dark Matter Searches at the LHC*, *JHEP* **01** (2014) 025, [[arXiv:1308.6799](#)].
- [51] G. Busoni, A. De Simone, J. Gramling, E. Morgante, and A. Riotto, *On the Validity of the Effective Field Theory for Dark Matter Searches at the LHC, Part II: Complete Analysis for the s -channel*, *JCAP* **1406** (2014) 060, [[arXiv:1402.1275](#)].
- [52] M. Endo and Y. Yamamoto, *Unitarity Bounds on Dark Matter Effective Interactions at LHC*, *JHEP* **06** (2014) 126, [[arXiv:1403.6610](#)].
- [53] G. Busoni, A. De Simone, T. Jacques, E. Morgante, and A. Riotto, *On the Validity of the Effective Field Theory for Dark Matter Searches at the LHC Part III: Analysis for the t -channel*, *JCAP* **1409** (2014) 022, [[arXiv:1405.3101](#)].
- [54] S. El Hedri, W. Shepherd, and D. G. E. Walker, *Perturbative Unitarity Constraints on Gauge Portals*, [arXiv:1412.5660](#).
- [55] N. F. Bell, Y. Cai, J. B. Dent, R. K. Leane, and T. J. Weiler, *Dark matter at the LHC: Effective field theories and gauge invariance*, *Phys. Rev.* **D92** (2015), no. 5 053008, [[arXiv:1503.07874](#)].
- [56] S. Baek, P. Ko, M. Park, W.-I. Park, and C. Yu, *Beyond the Dark matter effective field theory and a simplified model approach at colliders*, *Phys. Lett.* **B756** (2016) 289–294, [[arXiv:1506.06556](#)].
- [57] N. Bell, G. Busoni, A. Kobakhidze, D. M. Long, and M. A. Schmidt, *Unitarisation of EFT Amplitudes for Dark Matter Searches at the LHC*, [arXiv:1606.02722](#).

- [58] F. Kahlhoefer, K. Schmidt-Hoberg, T. Schwetz, and S. Vogl, *Implications of unitarity and gauge invariance for simplified dark matter models*, *JHEP* **02** (2016) 016, [[arXiv:1510.02110](#)]. [[JHEP02,016\(2016\)](#)].
- [59] U. Haisch, F. Kahlhoefer, and T. M. P. Tait, *On Mono-W Signatures in Spin-1 Simplified Models*, [arXiv:1603.01267](#).
- [60] C. Englert, M. McCullough, and M. Spannowsky, *S-Channel Dark Matter Simplified Models and Unitarity*, [arXiv:1604.07975](#).
- [61] J. M. Cline, G. Dupuis, Z. Liu, and W. Xue, *The windows for kinetically mixed Z' -mediated dark matter and the galactic center gamma ray excess*, *JHEP* **08** (2014) 131, [[arXiv:1405.7691](#)].
- [62] N. F. Bell, Y. Cai, and R. K. Leane, *Dark Forces in the Sky: Signals from Z' and the Dark Higgs*, *JCAP* **1608** (2016), no. 08 001, [[arXiv:1605.09382](#)].
- [63] M. Duerr, F. Kahlhoefer, K. Schmidt-Hoberg, T. Schwetz, and S. Vogl, *How to save the WIMP: global analysis of a dark matter model with two s-channel mediators*, [arXiv:1606.07609](#).
- [64] J. M. Cline, G. Dupuis, Z. Liu, and W. Xue, *Multimediatator models for the galactic center gamma ray excess*, *Phys. Rev.* **D91** (2015), no. 11 115010, [[arXiv:1503.08213](#)].
- [65] A. Choudhury, K. Kowalska, L. Roszkowski, E. M. Sessolo, and A. J. Williams, *Less-simplified models of dark matter for direct detection and the LHC*, [arXiv:1509.05771](#).
- [66] K. Ghorbani and H. Ghorbani, *Two-portal Dark Matter*, *Phys. Rev.* **D91** (2015), no. 12 123541, [[arXiv:1504.03610](#)].
- [67] M. Pospelov, A. Ritz, and M. B. Voloshin, *Secluded WIMP Dark Matter*, *Phys. Lett.* **B662** (2008) 53–61, [[arXiv:0711.4866](#)].
- [68] M. Pospelov and A. Ritz, *Astrophysical Signatures of Secluded Dark Matter*, *Phys. Lett.* **B671** (2009) 391–397, [[arXiv:0810.1502](#)].
- [69] M. Pospelov, *Secluded $U(1)$ below the weak scale*, *Phys. Rev.* **D80** (2009) 095002, [[arXiv:0811.1030](#)].
- [70] J. L. Feng, H. Tu, and H.-B. Yu, *Thermal Relics in Hidden Sectors*, *JCAP* **0810** (2008) 043, [[arXiv:0808.2318](#)].
- [71] J. L. Feng and J. Kumar, *The WIMPlless Miracle: Dark-Matter Particles without Weak-Scale Masses or Weak Interactions*, *Phys. Rev. Lett.* **101** (2008) 231301, [[arXiv:0803.4196](#)].
- [72] I. Z. Rothstein, T. Schwetz, and J. Zupan, *Phenomenology of Dark Matter annihilation into a long-lived intermediate state*, *JCAP* **0907** (2009) 018, [[arXiv:0903.3116](#)].
- [73] J. Mardon, Y. Nomura, and J. Thaler, *Cosmic Signals from the Hidden Sector*, *Phys. Rev.* **D80** (2009) 035013, [[arXiv:0905.3749](#)].
- [74] J. Mardon, Y. Nomura, D. Stolarski, and J. Thaler, *Dark Matter Signals from Cascade Annihilations*, *JCAP* **0905** (2009) 016, [[arXiv:0901.2926](#)].
- [75] P. Meade, M. Papucci, and T. Volansky, *Dark Matter Sees The Light*, *JHEP* **12** (2009) 052, [[arXiv:0901.2925](#)].
- [76] C. Cheung, G. Elor, L. J. Hall, and P. Kumar, *Origins of Hidden Sector Dark Matter I: Cosmology*, *JHEP* **03** (2011) 042, [[arXiv:1010.0022](#)].
- [77] H. Davoudiasl and I. M. Lewis, *Dark Matter from Hidden Forces*, *Phys. Rev.* **D89** (2014), no. 5 055026, [[arXiv:1309.6640](#)].

- [78] A. Berlin, P. Gratia, D. Hooper, and S. D. McDermott, *Hidden Sector Dark Matter Models for the Galactic Center Gamma-Ray Excess*, *Phys. Rev.* **D90** (2014), no. 1 015032, [[arXiv:1405.5204](#)].
- [79] J. Liu, N. Weiner, and W. Xue, *Signals of a Light Dark Force in the Galactic Center*, *JHEP* **08** (2015) 050, [[arXiv:1412.1485](#)].
- [80] E. Hardy, R. Lasenby, and J. Unwin, *Annihilation Signals from Asymmetric Dark Matter*, *JHEP* **07** (2014) 049, [[arXiv:1402.4500](#)].
- [81] C. Boehm, M. J. Dolan, and C. McCabe, *A weighty interpretation of the Galactic Centre excess*, *Phys. Rev.* **D90** (2014), no. 2 023531, [[arXiv:1404.4977](#)].
- [82] S. D. McDermott, *Lining up the Galactic Center Gamma-Ray Excess*, *Phys. Dark Univ.* **7-8** (2014) 12–15, [[arXiv:1406.6408](#)].
- [83] Z. Chacko, Y. Cui, S. Hong, and T. Okui, *Hidden dark matter sector, dark radiation, and the CMB*, *Phys. Rev.* **D92** (2015) 055033, [[arXiv:1505.04192](#)].
- [84] G. Elor, N. L. Rodd, and T. R. Slatyer, *Multistep cascade annihilations of dark matter and the Galactic Center excess*, *Phys. Rev.* **D91** (2015) 103531, [[arXiv:1503.01773](#)].
- [85] G. Elor, N. L. Rodd, T. R. Slatyer, and W. Xue, *Model-Independent Indirect Detection Constraints on Hidden Sector Dark Matter*, [[arXiv:1511.08787](#)].
- [86] M. Abdullah, A. DiFranzo, A. Rajaraman, T. M. P. Tait, P. Tanedo, and A. M. Wijangco, *Hidden on-shell mediators for the Galactic Center gamma-ray excess*, *Phys. Rev.* **D90** (2014) 035004, [[arXiv:1404.6528](#)].
- [87] A. Martin, J. Shelton, and J. Unwin, *Fitting the Galactic Center Gamma-Ray Excess with Cascade Annihilations*, *Phys. Rev.* **D90** (2014), no. 10 103513, [[arXiv:1405.0272](#)].
- [88] P. Ko and Y. Tang, *Dark Higgs Channel for FERMI GeV γ -ray Excess*, *JCAP* **1602** (2016), no. 02 011, [[arXiv:1504.03908](#)].
- [89] P. Ko, W.-I. Park, and Y. Tang, *Higgs portal vector dark matter for GeV scale γ -ray excess from galactic center*, *JCAP* **1409** (2014) 013, [[arXiv:1404.5257](#)].
- [90] Y. G. Kim, K. Y. Lee, C. B. Park, and S. Shin, *Secluded singlet fermionic dark matter driven by the Fermi gamma-ray excess*, [[arXiv:1601.05089](#)].
- [91] D. Hooper, N. Weiner, and W. Xue, *Dark Forces and Light Dark Matter*, *Phys. Rev.* **D86** (2012) 056009, [[arXiv:1206.2929](#)].
- [92] A. Berlin, S. Gori, T. Lin, and L.-T. Wang, *Pseudoscalar Portal Dark Matter*, *Phys. Rev.* **D92** (2015) 015005, [[arXiv:1502.06000](#)].
- [93] T. Kunimasa and T. Goto, *Generalization of the Stueckelberg Formalism to the Massive Yang-Mills Field*, *Prog. Theor. Phys.* **37** (1967) 452–464.
- [94] A. A. Slavnov, *Ward Identities in Gauge Theories*, *Theor. Math. Phys.* **10** (1972) 99–107. [*Teor. Mat. Fiz.*10,153(1972)].
- [95] M. J. G. Veltman, *Perturbation theory of massive Yang-Mills fields*, *Nucl. Phys.* **B7** (1968) 637–650.
- [96] A. A. Slavnov and L. D. Faddeev, *Massless and massive yang-mills field. (in russian)*, *Theor. Math. Phys.* **3** (1970) 312–316. [*Teor. Mat. Fiz.*3,18(1970)].
- [97] A. I. Vainshtein and I. B. Khriplovich, *On the zero-mass limit and renormalizability in the theory of massive yang-mills field*, *Yad. Fiz.* **13** (1971) 198–211.
- [98] K.-i. Shizuya, *Renormalization of Two-Dimensional Massive Yang-Mills Theory and Nonrenormalizability of Its Four-Dimensional Version*, *Nucl. Phys.* **B121** (1977) 125–140.

- [99] D. G. C. McKeon, *On using the Freedman-Townsend model to generate massive vectors*, *Can. J. Phys.* **69** (1991) 1249–1255.
- [100] D. Z. Freedman and P. K. Townsend, *Antisymmetric Tensor Gauge Theories and Nonlinear Sigma Models*, *Nucl. Phys.* **B177** (1981) 282–296.
- [101] Yu. N. Kafiev, *Massive Yang-Mills Fields: Gauge Invariance and One Loop Counterterm*, *Nucl. Phys.* **B201** (1982) 341–351.
- [102] **Particle Data Group** Collaboration, K. A. Olive et al., *Review of Particle Physics*, *Chin. Phys.* **C38** (2014) 090001.
- [103] G. Belanger, F. Boudjema, A. Pukhov, and A. Semenov, *micrOMEGAs 3: A program for calculating dark matter observables*, *Comput. Phys. Commun.* **185** (2014) 960–985, [[arXiv:1305.0237](#)].
- [104] **Planck** Collaboration, P. A. R. Ade et al., *Planck 2013 results. XVI. Cosmological parameters*, *Astron. Astrophys.* **571** (2014) A16, [[arXiv:1303.5076](#)].
- [105] S. Weinberg, *Goldstone Bosons as Fractional Cosmic Neutrinos*, *Phys. Rev. Lett.* **110** (2013), no. 24 241301, [[arXiv:1305.1971](#)].
- [106] A. Djouadi, J. Kalinowski, and M. Spira, *HDECAY: A Program for Higgs boson decays in the standard model and its supersymmetric extension*, *Comput. Phys. Commun.* **108** (1998) 56–74, [[hep-ph/9704448](#)].
- [107] G. Steigman, B. Dasgupta, and J. F. Beacom, *Precise Relic WIMP Abundance and its Impact on Searches for Dark Matter Annihilation*, *Phys. Rev.* **D86** (2012) 023506, [[arXiv:1204.3622](#)].
- [108] J. Ellis, *TikZ-Feynman: Feynman diagrams with TikZ*, [[arXiv:1601.05437](#)].
- [109] A. Alves, A. Berlin, S. Profumo, and F. S. Queiroz, *Dark Matter Complementarity and the Z' Portal*, *Phys. Rev.* **D92** (2015), no. 8 083004, [[arXiv:1501.03490](#)].
- [110] A. Alves, A. Berlin, S. Profumo, and F. S. Queiroz, *Dirac-fermionic dark matter in $U(1)_X$ models*, *JHEP* **10** (2015) 076, [[arXiv:1506.06767](#)].